Experimental Investigation of Liquid Distribution Over Structured Packing

S. V. Alekseenko, D. M. Markovich, A. R. Evseev, A. V. Bobylev, B. V. Tarasov, and V. M. Karsten
Institute of Thermophysics SB RAS, Novosibirsk 630090, Russia

DOI 10.1002/aic.11498
Published online April 25, 2008 in Wiley InterScience (www.interscience.wiley.com).

The thickness of a liquid film on the structured packing inside a distillation column was measured at the region of counter-current flow of gas and liquid by fiber-optic sensors. The local distribution of liquid inside a typical geometrical cell formed by the corrugated Koch 1Y sheets was examined in this study. It is shown that, in the vicinity of the sheet contact points inside the cell, the liquid film thickness is maximal, and peculiar meniscuses are formed where liquid flow redistribution over the corrugation surface occurs. A counter gas flow decreases pulsations of the liquid film thickness by a factor of 1.5–2 on the rib and lateral surfaces of corrugation. Experimental data on the effect of operation parameters on the local distribution of liquid in the cell and the pressure drop in the column are presented. © 2008 American Institute of Chemical Engineers *AIChE J,* 54: 1424–1430, 2008
Keywords: distillation, films, fibers, fluid mechanics, multi-phase flow

Introduction

Application of structured packing in columns increases the efficiency of the absorption and distillation processes. A special shape of the packing with a doubled structure of corrugation enlarges the specific geometrical surface of the sheets by up to 500–750 m^2/m^3 and more. This increases the interface surface and productivity of industrial boilers. Thus, despite a relatively high cost, the regular packings are widely used in chemical, food, oil, and other industries.[1–4]

There are various inner geometrical characteristics of the regular packing setup in industry; their configurations and arrangements have been shown in different papers.[5–8] The main advantages of these packings are small pressure drop values and a high productivity and efficiency.

The efficiency of mass transfer processes in such columns is connected directly with liquid spreading and the distribution over the interface surface inside the packing. The geometrical characteristics of the regular packing, the physical properties of liquid and packing material, and other factors affect the liquid distribution inside the column, and this has been the subject of other studies.[5,9–14] Experimental data on the effect of the operation parameters on the pressure drop, mass transfer efficiency, and distribution of the local flow parameters in a distillation column with a 0.9-m diameter and a regular aluminum Koch 1Y packing are shown in Pavlenko et al.[12,13]

It is shown by Nicolaiewsky et al.[14] and Nicolaiewsky and Fair[15] that for the vertical plane sheets a decrease in surface tension and contact angle improves liquid spreading and surface wetting both for standard and corrugated sheets. The surface texture and roughness of a sheet also improve its wetting at the expense of contact angle reduction. A rise of liquid viscosity provides the formation of the thicker films and inhibits film spreading over the sheet surface.

The film flow of a viscous liquid over an inclined corrugated surface is considered by Trifonov.[16] Calculations are carried out in a wide range of Reynolds numbers and geometrical characteristics of the surface. It is shown that in the case of a single-dimensional surface there is a range of parameters where the flow is mainly determined by surface tension; for the surfaces with a double corrugation, the averaged flow characteristics at a large embossing are determined by a small texture geometry. It is shown in Zhao and Cerro[17] that the flow of a viscous film over a corrugated surface is determined by the Reynolds number and the capillary number.

Correspondence concerning this article should be addressed to A. V. Bobylev at bobylev@itp.nsc.ru.

The structure and flow modes of the film above a corrugated wall were studied by Vlachogiannis and Bontozoglou.[18]

The method of X-ray computer tomography is suggested by Marchot et al.[19] for the investigation of the liquid distribution inside a structured packing (with localization of about 1 mm) and for commercial packing testing.

According to an analysis of the papers, the mechanism of liquid distribution in the column, filled with the structured packing, is studied insufficiently. It is necessary to determine the interconnection between the local hydrodynamic characteristics of liquid and gas flows and integral parameters of column operation. The flows of the liquid in a small-scale area (elementary cell) significantly effect the large-scale distribution. Inside a cell, the distribution of liquid is determined by its flow across the rib crests, contact points, and holes in the elements of the corrugated sheets. There is no experimental data on the effect of the operation parameters on the local distribution of liquid inside a typical geometrical cell that is formed in the regular packing and located in-between the adjacent contact points of the corrugated sheets.

This work is aimed at providing experimental study of the local liquid distribution inside a typical geometrical cell and the effect of operation parameters on this distribution and pressure drop in the column with the structured Koch 1Y packing.

Experiments

Experiments were carried out in the organic glass model of the distillation column, with a height of 2 m and a cross-section of 0.2×0.2 m^2. The effect of the operation parameters on the local distribution of liquid over the corrugated surfaces inside a geometrical regular cell was studied together with the pressure drop in the column in the presence of the counter-current flow of liquid and air. Distilled water ($\rho_L = 1.0 \times 10^3$ kg/m^3, $\mu = 1.002 \times 10^{-3}$ Pa·s, $\sigma_L = 0.0727$ N/m) and rectified ethanol ($\rho_L = 0.83 \times 10^3$ kg/m^3, $\mu = 1.2 \times 10^{-3}$ Pa·s, $\sigma_L = 0.0223$ N/m) were used as the working fluid in these experiments.

The scheme of the experimental setup is shown in Figure 1. The working fluid was pumped from a receiving tank into a constant header tank, located at a height of 7 m. Liquid from this tank passed through a flow sensor and regulation valve into the distributor, where the liquid jets were formed by 39 nozzles with holes 2.3×10^{-3} m in diameter. For the hexagonal pattern, the distance between nozzles was 3.5×10^{-2} m. Within the operation area, the liquid jet irrigated the mass-transfer packing, which was assembled by corrugated sheets. The distance between the distributor and the edge of the upper plug was 0.2 m. Then, liquid flowed into the receiving vessel through the separator-distributor and distributing boiler. The separator-distributor was constructed according to the principle of a hydraulic gate.

Air from the gas main was fed through a filter and flow sensor into the separator-distributor, and then supplied into the working part of the column. Within the working part, air traveled along the grooves, formed by the large corrugation, and through 3-mm diameter holes, which were distributed uniformly over the corrugated sheets. After the working part, air passed through special holes in the distributor and was released into the atmosphere. The direction of the liquid and air flows, the setup for measurement of the local liquid film thickness by a fiber-optic sensor, and a standard sensor for pressure drop, are shown in Figure 1 by solid and dashed arrows.

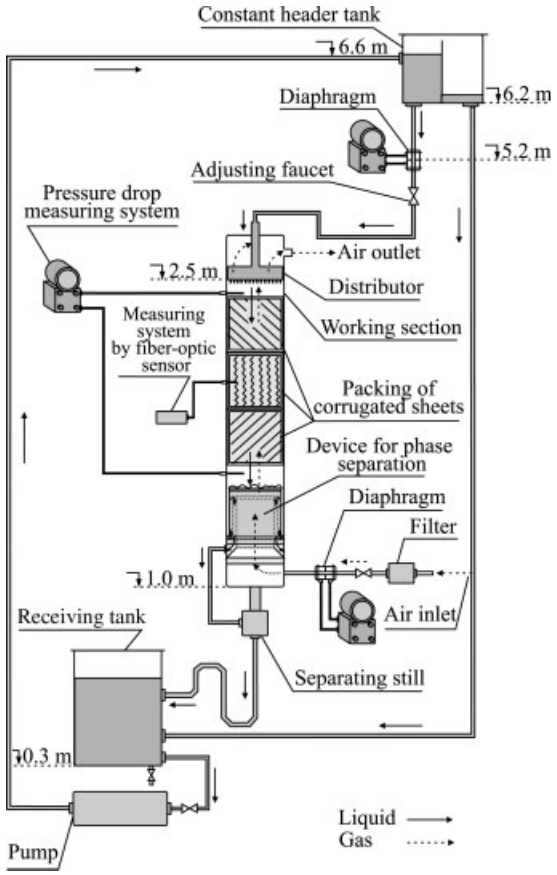

Figure 1. Scheme of the experimental setup.

As it is known, the area of the specific geometrical surface of the packing can be varied over a large range by alteration of the geometrical characteristics of embossing. In these experiments, the Koch 1Y packing with a specific geometrical area of 435 m^2/m^3 was tested. It consists of the structure-forming elements, which occupy the whole cross-section of the column. Adjacent elements are oriented at an angle of 90° relative to each other. Each element consists of parallel corrugated aluminum sheets with a thickness of 3×10^{-4} mm and 0.195×0.2 m^2 size. The corrugation is made at a fixed angle $\Psi = 45°$ relative to the vertical axis and, at adjacent sheets, they are directed toward the opposite sides of the column. The corrugated period is 1.4×10^{-2} m, and the period of the small-scaled horizontal texture is 1.85×10^{-3} m.

It is shown by Nicolaiewsky et al.[14] that a decrease in surface tension and contact angle improves surface wetting by a liquid. Therefore, the corrugated aluminum sheets were treated by the electrochemical method.[20] At that, a distilled water droplet was spread over the aluminum surface uniformly, similar to ethanol, at the expense of a decrease in the contact angle by ~(20–30)%; also, ethanol spreading became more stable in these experiments.

The liquid flow rate in these experiments was changed from 0.05 to 0.5 l/s, which corresponded to a liquid loading

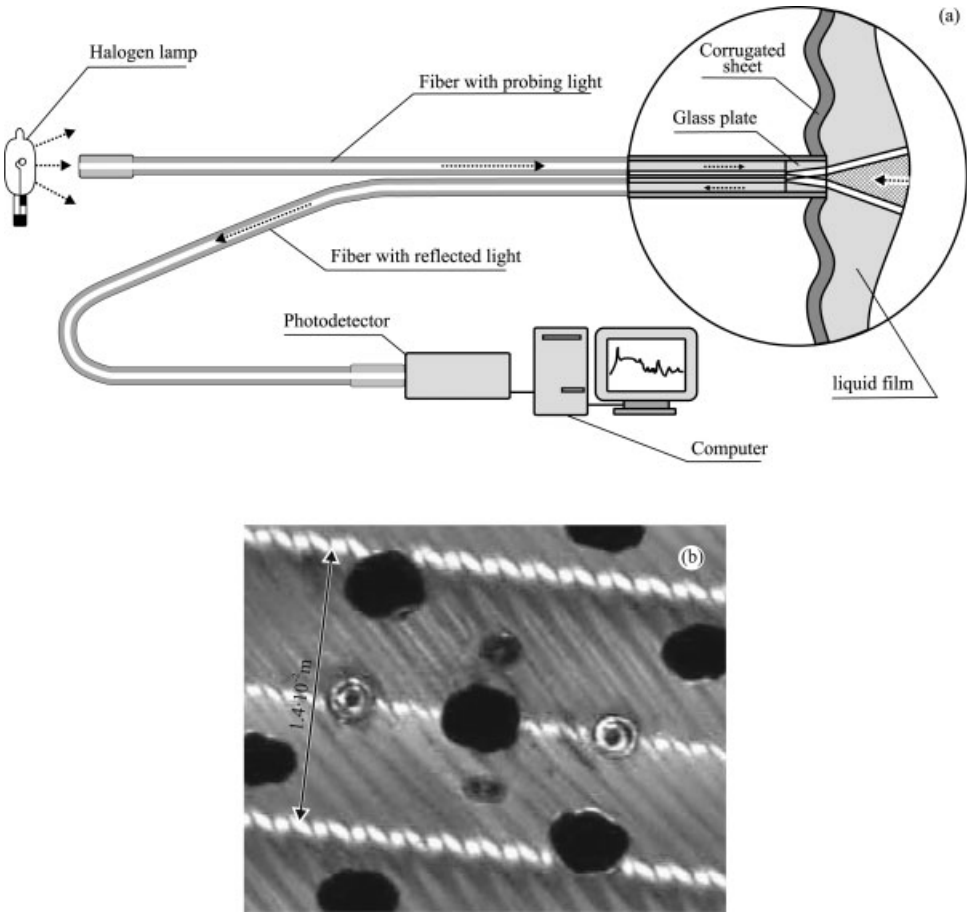

Figure 2. Block diagram of measurement channel (a) and a picture of the corrugated Koch 1Y sheet with sensors (b).

factor $C_L = U_L \times [\rho_L/(\rho_L-\rho_V)]^{0.5} = (1.25–12.5) \times 10^{-3}$ m/s. In calculations done per nozzle, the liquid flow rate was changed from 1.3 to 13 ml/s. The factor of the column loading by air was $K_V = U_V \times [\rho_g/(\rho_L-\rho_V)]^{0.5} = (0.006–0.06)$ m/s, which corresponded to an air flow rate from 6 to 60 l/s. Here U_L and U_V are the liquid and air velocities reduced to the column cross-section, and ρ_L, ρ_V are the densities of liquid and air, respectively. The ratio of the mass flow rates of phases (m_V /m_L) ranged from 0.015 to 1.5.

To diagnose different flows of phases in the column, the multichannel measurement system, consisting of four standard pressure sensors and four fiber-optic sensors of the reflection type, was developed. A special application for OS Windows, providing acquisition, presentation, and treatment of experimental data in real time, was developed. The following values were measured in the experiments: liquid and air flow rates, pressure drop in the column; local thickness of a liquid film over the corrugated surface, both averaged in time and its pulsation characteristics. Besides, the probability of a liquid film or a dry spot existence for the vicinity of probes location was obtained for studies regimes.

The scheme of the measurement channel of the fiber-optic sensor (a) and the picture of corrugated Koch 1Y sheet with four sensors mounted at the level of fine texture crests (b) are shown in Figure 2. The operation principle is as follows. Light from a halogen lamp of the 100-W power was sent through a probing light guide into the studied zone of the liquid film. Light, reflected from the film, was sent through the receiving light guide to an avalanche photodiode. The diameter of a probing light spot on the liquid film surface did not exceed $(3–4) \times 10^{-4}$ m. An electron signal from a photodetector was sent to a PC. In contrast to a standard two-fiber sensor,[8] a glass sheet (3) with a thickness of 2×10^{-3} m was glued on the modified fiber-optic sensor. This way, the ambiguity between the film thickness and the electric signal of the two-fiber sensor was eliminated. The method of film thickness measurement by means of a fiber-optic sensor is described in detail by Krohn[21] and Evseev.[22] The liquid film thickness δ was calculated in real time by the electric signal of the fiber-optic sensor at the PC, using a special program that considers the results of each sensor static calibration.

Investigation Results

The dependence of the reduced pressure drop in the column ΔP (Pa/m) on the F-factor is shown in Figure 3 for three liquid flow rates, where $F = U_V \times (\rho_V)^{0.5}$. Solid lines in the diagram (Curve 1, 2, 3) indicate measurements of ΔP for water and ethanol; they almost coincide. The error of the ΔP measurement in the experiments was $(\pm 5)\%$. According

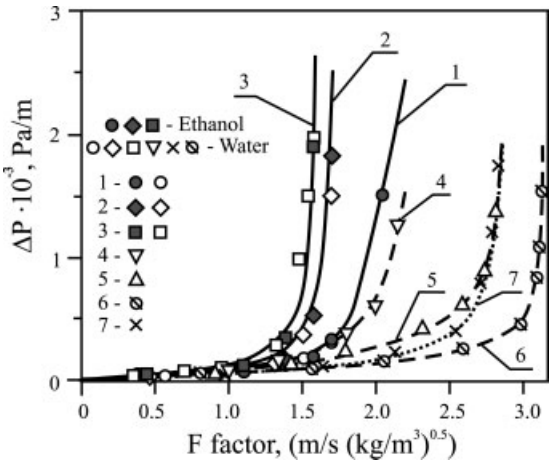

Figure 3. Pressure drop in the column for different flow rates of gas and liquid.

With corrugated Koch 1Y sheets, $C_L = 0.25 \times 10^{-2}$ m/s (Curve 1); $C_L = 0.75 \times 10^{-2}$ m/s (Curve 2); $C_L = 1.25 \times 10^{-2}$ m/s (Curve 3); with corrugated Mellapak 250Y sheets, at $d = 0.3$ m, (Meier et al.,[25]), $C_L = 1.67 \times 10^{-2}$ m/s, (Curve 4); $C_L = 1.12 \times 10^{-2}$ m/s, (Curve 5); with corrugated Mellapak 250X sheets, at $d = 1.0$ m, (Suess P. and L. Spiegel[24]), $C_L = 2.08 \times 10^{-2}$ m/s, (Curve 6); $C_L = 2.8 \times 10^{-2}$ m/s, (Curve 7).

to visual observations, a drastic increase in ΔP is caused by the transition of the counter-current liquid and gas flow into the flooding mode. In most experiments, this mode started to develop from film breakup at the lowest element of the packing. Then, with a small increase in the gas velocity, flooding rapidly propagated upward to all elements until complete "flooding" in the column. The measurements have shown that, with an increase in the liquid flow rate, the transition to the flooding mode occurred at relatively lower gas flow rates. It is possible that relatively thicker liquid films can be easily removed from the structured packing by a counter-current gas flow.

Similar results for a column of 0.3-m diameter with corrugated Sulzer Mellapak 250Y sheets[25] are shown in the diagram for comparison (Curve 4, 5), together with the data for the 1-m column with Sulzer Mellapak 250X sheets[23] (Curve 6, 7), obtained at the counter-current flow of water and air. As we can see, the pressure drop ΔP in the mentioned columns is significantly less, and the transition to the flooding mode starts at a higher F-factor. These differences can be explained by a larger contact area of the tested Koch IY sheets, which has a specific geometrical area that is significantly larger than that of the Sulzer Mellapak 250Y and Sulzer Mellapak 250X sheets. For the distillation processes, the Sulzer Brasers Ltd. (Winterthur, Switzerland) Company has developed several types of commercial packing, including the Mellapak, whose operation characteristics are presented in Shpigel and Mayer[5] for four types of packing: 125Y, 250Y, 350Y, and 500Y. The commercial Koch 1Y packing has almost the same characteristics as the Mellapak 500Y. The reference designation of the packing type includes two geometrical parameters: Y is the value of the angle $\Psi = 45^\circ$, and the number is the specific geometrical area of the packing in m^2/m^3.

The model for the calculation of the pressure drop in the column, using the analogy of a gas flow along tubes, is offered by Brunazzi and Paglianti.[26] This model assumes that the pressure drop is determined by the friction of gas flowing along the channels of a structured packing as along a tube. The liquid phase, occupying some part of space, reduces the packing cross-section for the gas phase, affecting the pressure drop in the column. This approach to analyzing the results of the pressure drop in the column can be useful for hydraulic modes without flooding.

The flow field of the liquid and gas inside the plugs of regular sheets can be divided into similar geometrical cells whose key elements include corrugation geometry and contact points between the sheets and the holes. Therefore, experimental studies on the local distribution of liquid at the counter gas flow can be carried out inside a single geometrical cell. It can be assumed that, in geometrically similar cells inside the working plugs of corrugated sheets, the local distributions of liquid will be identical. Our measurements were carried out at the phase flow without flooding.

It is known that the processes of liquid flow in cells, which determine the liquid flow across the rib crests, contact points, and holes in every element, significantly affect the large-scale distribution. However, there are no published quantitative characteristics of the liquid flow in the cell and profiles of the liquid film thickness.

Let's consider the mechanism of liquid distribution in a boundary cell, which is available for observation and video recording, at the irrigation of an element of 10 corrugated sheets of the Koch 1Y by a single jet of ethanol. The flow rate of ethanol was 4×10^{-6} m^3/s. The jet flowed from a nozzle with a 2.3×10^{-3} m diameter from a height of 7×10^{-2} m above the element center. The typical pattern of

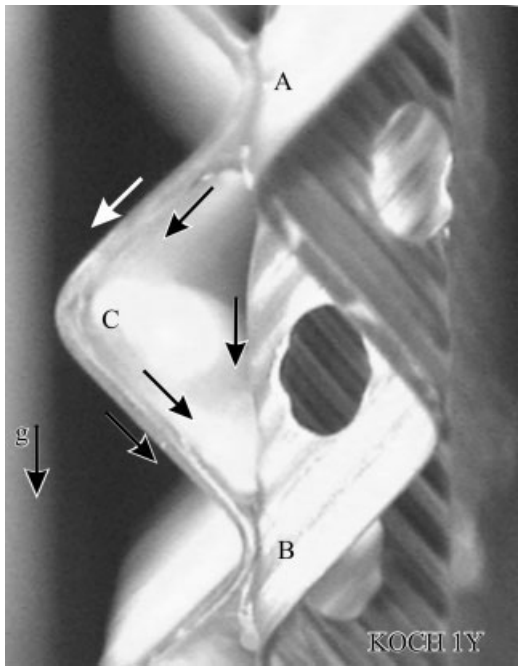

Figure 4. Spreading of ethanol film over a boundary geometrical cell on the Koch 1Y sheet.

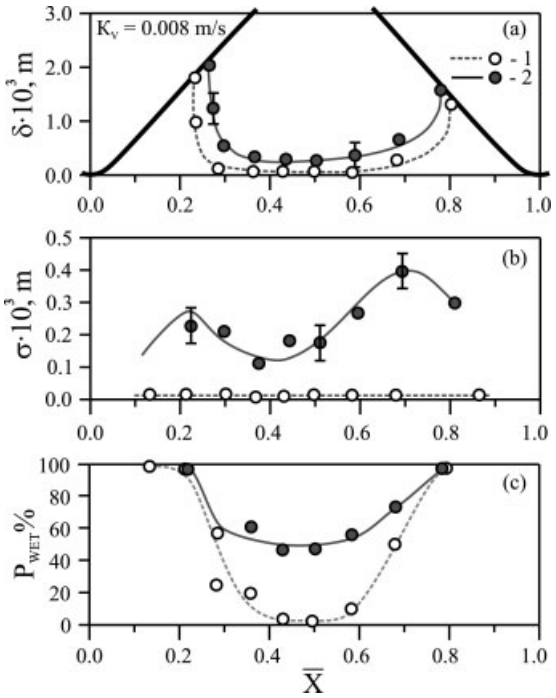

Figure 5. Ethanol film thickness on a rib between adjacent contact points in the central cell (a), root-mean-square pulsations of the film thickness (b) and probability of liquid presence (c) at K_V = 0.008 m/s and C_L = 0.005 m/s (1), C_L = 0.015 m/s (2).

liquid distribution in a boundary cell over the corrugated sheet surface is shown in Figure 4. According to visual observations made near every contact point on the ribs of corrugated sheets (e.g., points *A* and *B*), the liquid forms two peculiar related meniscuses, where the film thickness is maximal, but not identical. The lower "ceiling" meniscus is larger than the upper "bottom" one because of the liquid downflow under the action of gravity. Further down the flow, liquid from meniscus *A* flows mainly over the lateral surface under the action of Coand's effect, forming a third meniscus *C* inside a dihedral angle of corrugation. Some part of the liquid flows over a rib. It can be assumed that this mechanism of liquid redistribution occurs at every contact point of corrugated sheets inside each element.

Measurements of the liquid film thickness δ by a fiber-optic sensor, its RMS pulsations σ, and the probabilities of liquid presence on the corrugated sheets (P_{wet}) were carried out inside a cell in the center of the working part of the column equipped with three elements, i.e., in the geometrical middle of the second element.

The factors of column loading by ethanol and air in these experiments were: $C_L = (2.5–15) \times 10^{-3}$ m/s and $K_V = (0.008–0.035)$ m/s. The results of measurements on a rib inside the central cell are shown in Figure 5a,b,c (K_V = 0.008 m/s) for two flow rates of liquid. Here $\overline{X}$ is a dimensionless distance along a rib between contact points of the sheets. The step between the sheet ribs $\lambda = 1.4 \times 10^{-2}$ m was chosen as a scale along the axis *X*, i.e., $\overline{X} = X/\lambda$. Coordinates of a measurement point on a rib were changed by the choice (shift) of an adjacent sheet for the same sheet with glued fiber-optic sensors. For a low liquid flow rate (Figure 5a, $C_L = 5 \times 10^{-3}$ m/s) in the central cell, the rib is dry, the "ceiling" meniscus ($\overline{X} \approx 0.22$) is slightly larger than the "bottom" meniscus $\overline{X} \approx 0.78$), and the intensity of pulsations of the film thickness σ (Figure 5b) is almost zero. The probability profile of the liquid film presence P_{wet} on a rib (Figure 5c) has the shape of a trench. Near the points of the sheet contact, liquid in the menisci is always available with a probability of 100%, and the film thickness is maximal. In the central zone of a rib, P_{wet} is almost zero. It should be noted that the fiber-optic sensor was mounted at the level of the crests of the fine horizontal texture. At that, a very thin liquid film could streamline the sensor without wetting its sensitive glass surface.

An increase in the liquid flow rate at K_V = 0.008 m/s (Figure 5a, $C_L = 1.5 \times 10^{-2}$ m/s) provides an insignificant rise of the menisci and the generation of a thin liquid film in the center of a rib. The profile of RMS pulsations σ (Figure 5b) has two maxima, which are located near the meniscus boundaries. Pulsation intensity near the "bottom" meniscus is almost twice as high as that of the "ceiling" meniscus, which indicates the more intensive process of liquid redistribution in this zone of the rib inside a cell. Thus, the probability of liquid film formation P_{wet} in the central zone of the rib increases up to ~55% (Figure 5c).

An increase in the gas flow rate in the column (K_V = 0.035 m/s) provides a slight redistribution of liquid inside a cell and some leveling of meniscuses together with the formation of a thin film in the rib center at $C_L = 5 \times 10^{-3}$ m/s (Figure 6a). The intensity of the liquid film pulsations over the whole length of a rib becomes uniform, and the amplitude decreases by a factor of two (Figure 6b). The gas flow stabilizes the liquid film. Thus, the probability profile P_{wet} on the rib changes slightly (Figure 6c).

Therefore, the distribution of liquid over a rib inside the central geometrical cell corresponds qualitatively to results of visual studies of the liquid distribution inside a boundary cell (see Figure 4).

Distributions of the liquid film thickness and its RMS pulsations in a valley and over the lateral surfaces of corrugation in the central cell vs. operation parameters are shown in Figure 7a,b for K_V = 0.009 m/s. It is shown in Figure 7a that, with a rise of the liquid flow rate, the film thickness increases gradually in the cell valley (Curve 1) and over the lateral surfaces of corrugation (Curve 2, 3). On the "bottom" surface of corrugation (Curve 2), the film thickness is (10–20)% less than that on the "ceiling" surface (Curve 3). Pulsations of the liquid film thickness in the valley and over lateral surfaces of corrugation equal zero up to $C_L \approx 7.5 \times 10^{-3}$ m/s. A rise of C_L up to 5×10^{-3} m/s leads to a growth of σ of up to ~$(5–6) \times 10^{-4}$ m on the lateral surfaces of corrugation and, in the valley, it reaches ~5×10^{-5} m (Figure 7b). The flow over the lateral surfaces of corrugation is less stable than in the valley, which is probably connected with the process of liquid flow across the corrugation ribs.

An increase in the gas flow rate in the column up to K_V = 0.0273 m/s provides the growth of the liquid film thickness in the cell valley by (10–20)% (Figure 8a). On the "ceiling" surface of corrugation, the film thickness also increases by

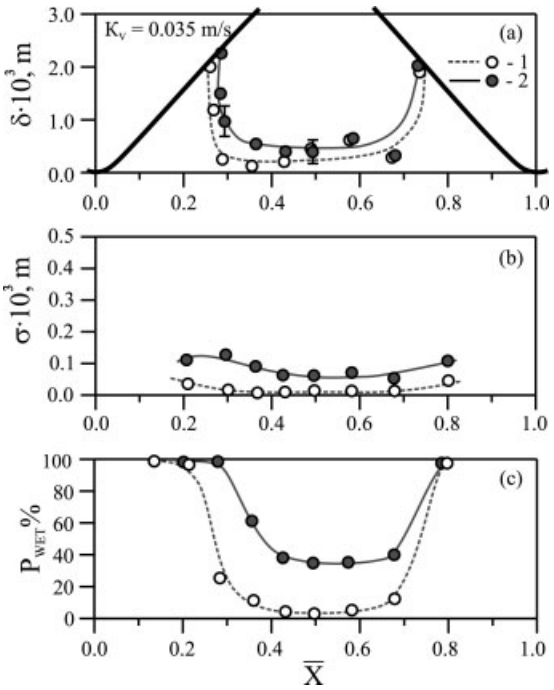

Figure 6. Ethanol film thickness on a rib between adjacent contact points in the central cell (a), root-mean-square pulsations of the film thickness (b) and probability of liquid presence (c) at K_V = 0.035 m/s and C_L = 0.005 m/s (1), C_L = 0.015 m/s (2).

(10–20)%, and on the "bottom" surface of corrugation, it decreases insignificantly (Figure 8a). The intensity of film thickness pulsations on the lateral surfaces of corrugation decrease almost by a factor of two, i.e., the effect of film surface stabilization by the counter air flow is observed (Figure 8b).

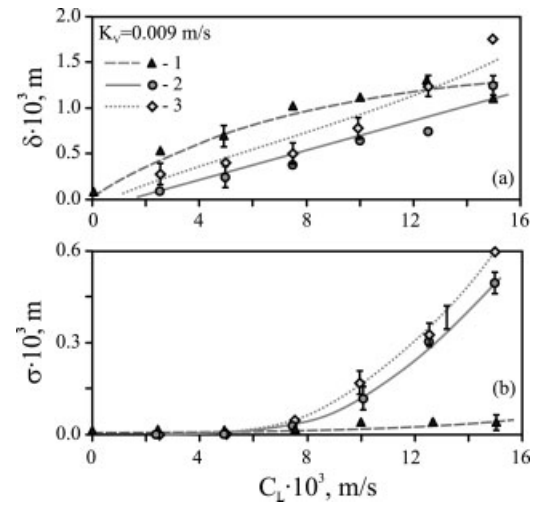

Figure 7. Dependence of film thickness (a) and root-mean-square pulsations of the liquid film thickness (b) on C_L at K_V = 0.009 m/s; valley (1), bottom slope of corrugation (2), ceiling slope of corrugation (3).

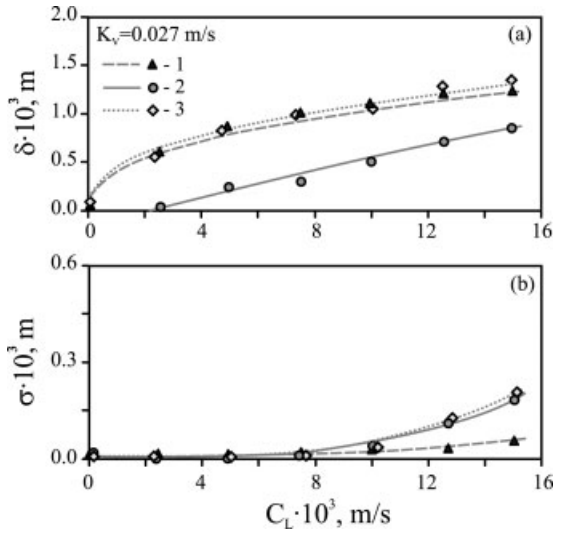

Figure 8. Dependence of film thickness (a) and root-mean-square pulsations of the liquid film thickness (b) on C_L at K_V = 0.027 m/s; valley (1), bottom slope of corrugation (2), ceiling slope of corrugation (3).

According to the analysis of the experimental results, the film thickness near the contact points changed slightly at the liquid flow rate reduction. With a rise of the liquid flow rate, these changes are more significant, i.e., hysteresis is observed at liquid spreading over a corrugated sheet, as by Nicolaiewsky et al.[14] The measurement results at a decreased flow rate are taken as a basis because of their stability. According to our observations, the liquid near the contact points moves—it is not stable. A comparison of the film thickness near the contact points, in valleys and slopes of corrugation, demonstrates that at relatively low flow rates the amount of liquid passing through the contact points is almost the same as that flowing along the valleys of a corrugated sheet.

The distribution of ethanol film thickness over the column cross-section in the middle of the second plug is shown in Figure 9 for $C_L = 1.5 \times 10^{-2}$ m/s and $K_V = 0.008$ m/s. Here, r is a transverse coordinate and $R = 0.1$ m is half of the distance between the lateral column walls. The transverse coordinate r

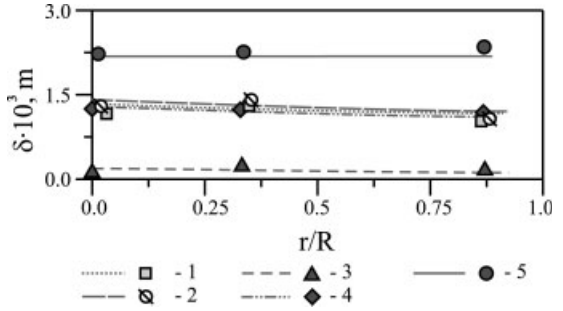

Figure 9. Distribution of the liquid film thickness over the column cross-section at C_L = 0.015 m/s and K_V = 0.077 m/s.

Bottom slope of corrugation (1), ceiling slope of corrugation (2), rib center (3), valley (4), contact points (5).

was changed at the stage of element reassembling and installation of two adjacent sheets with the sensors at different distances from the column wall. The typical film thicknesses near the contact points between the sheets (menisci) and in the central zone of a rib change insignificantly over the column cross-section. In a valley and over the lateral surfaces of corrugation inside a cell, the film thicknesses decrease slightly in the near-wall zone of the column.

Conclusions

A method for the measurement of liquid film thickness on corrugated sheets inside a column with a regular packing using a fiber-optic sensor has been developed.

It is shown that inside a typical geometrical cell, the maximal thickness of a liquid film is near the contact points of the sheets, where liquid is redistributed over the corrugated surface.

An increase in the liquid flow rate elicits growth of the film thickness mainly in valleys and on the lateral surfaces of corrugation inside a cell. An increase in the gas flow rate provides insignificant redistribution of liquid inside a cell and reduction in pulsations of the film thickness by a factor of 1.5–2 on a rib and lateral surfaces of corrugation.

Over the cross-section, the liquid film thickness near the sheet contact points and on a rib stays almost constant; in valleys and on the lateral surfaces of corrugation, it decreases insignificantly near the column wall.

The mode of film detachment from corrugated sheets by the counter air flow up to complete flooding is accompanied by a drastic increase in the pressure drop in the column.

Acknowledgments

The work was supported by the grant of the leading scientific schools No. NSh-6749.2006.8, and by the Air Products and Chemicals, Inc. (USA).

Notation

C_L = factor of column loading by liquid, m/s
K_V = factor of column loading by gas, m/s
m_V, m_L = mass flow rates of gas and liquid, kg/s
P_{wet} = probability of the liquid film presence, %
Q_L, Q_V = volumetric flow rates of liquid and gas, m^3/s
S = area of the column cross-section, m^2
$U_L = Q_L/S$, liquid velocity normalized by the column cross-section, m/s
$U_V = Q_V/S$, gas velocity normalized by the column cross-section, m/s
$\overline{X}$ = dimensionless distance along a rib between the adjacent contact points of sheets
$\overline{\delta}$ = liquid film thickness, averaged in time, m
ρ_L, ρ_V = densities of liquid and air, kg/m^3
μ = liquid viscosity, Pa·s
σ_L = coefficient of liquid surface tension, N/m
$\sigma = (\overline{\delta}^2 - \delta^2)^{0.5}$ = root-mean-square deviation of the liquid film thickness, m
$\lambda = 1.4 \cdot 10^{-2}$ m = distance between the ribs of corrugated sheets, m
$F = U_V \cdot (\rho_V)^{0.5}$ = F-factor, $(m/s) \cdot (kg/m^3)^{0.5}$
U, U_m = operation and maximal voltage of the fiber-optic sensor, V
ΔP = pressure drop in the column, Pa/m

Literature Cited

1. Kister HZ. *Distillation Design*. New York: McGraw-Hill, 1992.
2. Kalbassi MA, Zone I. Large Industrial-Scale Demonstration of Structured Packing Distillation System. In: *Proceedings of International Congress on Process Industries Achem*. Mexico City, America, March 18–20, 2002.
3. Stichlmair JL, Fair JR. *Distillation, Principles and Practices*. New York: Wiley-VCH, 1998.
4. Carey VP. *Liquid-Vapor Phase-Change Phenomena*. London: Hemisphere, 1992, 95.
5. Spiegel L, Mayer W. Characteristics of various Mellapack packing operation. *Khimicheskoe i neftyanoe mashinostroenie*. 1994;3:16.
6. Strigle RF Jr. *Packed Tower Design and Applications: Random and Structured Packing*. Houston, TX: Gulf Publications, 1994.
7. Gunn DI, Al-Saffar HBS. Liquid distribution in packed column. *Chem Eng Sci*. 1993;48:3845.
8. Olujic Z, Seibert AF, Fair JR. Influence of corrugation geometry on the performance of structured packings: an experimental study. *Chem Eng Process V*. 2000;39:335.
9. Olujic Z, Kamerbeek AB, de Graauw J. A corrugation geometry based model for efficiency of structured distillation packing. *Chem Eng Process*. 1999;38:683.
10. Spiegel L, Meier W. Distillation column with structured packing in the next decade. In: *Proceedings of International Conference of Distillation and Absorption*. Baden-Baden, Germany, 30 Sept–2 Oct, 2002.
11. Behrens M, Saraber PP, Yamsen H, Olujic Z. Performance characteristics of a monolith-like structured packing. *Chem Biochem Eng Q*. 2001;15:49.
12. Pavlenko AN, Pecherkin NI, Chekhovich VYu, Zhukov VE, Sunder S, Houghton P, Serov AF, Nazarov AD. Large industrial-scale model of structured paking distillation column. *J Eng Thermophys*. 2005; 13:1.
13. Pavlenko AN, Pecherkin NI, Chekhovich VYu, Zhukov VE, Sunder S, Houghton P, Serov AF, Nazarov AD. Separation of mixtures and liquid distribution over the structured packing of the large-scaled model of a distillation column. *Theory Found Chem Eng*. 2006;40:4.
14. Nicolaiewsky EMA, Tavares FW, Rajagopal K, Fair JR. Liquid film flow and area generation in structured packing columns. *Powder Tech*. 1999;104:84.
15. Nicolaiewsky EMA, Fair JR. Liquid flow over textured surfaces. 1. contact angles. *Ind Eng Chem Res*. 1999;38:284.
16. Trifonov YY. Viscous film flowing over the corrugated surfaces. *J Appl Mech Tech Phys*. 2004;45:97.
17. Zhao L, Cerro RL. Experimental characterization of viscous film flows over complex surfaces. *Int J Multiphase Flow*. 1992;18:495.
18. Vlachogiannis M, Bontozoglou V. Experiments on laminar film flow along a periodic wall. *J Fluid Mech*. 2002;457:133.
19. Marchot P, Toye D, Pelsser A-M, Crine M, L'Homme G, Olujic Z. Liquid distribution images on structured packing by x-ray computed tomography. *AIChE J*. 2001;47:1471.
20. Volosatov VA. *Hand-Book on Electrochemical and Electrophysical Methods of Treatment*. Leningrad: Mashinostroenie, 1988, 719.
21. Krohn DA. Fiberoptic and laser sensor IV. *SPIE*. 1986;718:2.
22. Evseev AR. Liquid film thickness measurement by the fiber optical probe. In: *Proceedings of the International Symposium on the Physics of Heat Transfer in Boiling and Condensation*. Moscow, Russia, May 21–24, 519, 1997.
23. Meier W, Hunkeler R, Stocker WD. Sulzer Mellapak-Eine Neue, *Geordnete Packung fur Stoffaustausch-Apparate Chem-Ing-Tech*. 1979; 51:119.
24. Suess P, Spiegel L. Holdup of Mellapak Structured Packings. *Chem Eng Process*. 1992;31:119.
25. Alekseenko SV, Bobylev AV, Evseev AR, Karsten VM, Markovich DM, Tarasov BV. Measurement of the liquid film thickness by the fiber-optic sensor. *Instr Exp Tech*. 2003;2:130.
26. Brunazzi E, Paglianti A. Mechanistic Pressure Drop Model for Columns Containing Structured Packings. *AlChE J*. 1997;43:317.

Manuscript received Aug. 16, 2007, revision received Dec. 30, 2007, and final revision received Feb. 27, 2008.